Article

Chinese Science Bulletin

Geology

November 2013 Vol.58 No.32: 3922–3936
doi: 10.1007/s11434-013-5926-8

Structural and chronological constraints on a Late Paleozoic shortening event in the Yanshan Tectonic Belt

LIN ShaoZe*, ZHU Guang, YAN LeJia, SONG LiHong & LIU Bei

School of Resource and Environmental Engineering, Hefei University of Technology, Hefei 230009, China

Received February 21, 2013; accepted May 7, 2013; published online June 6, 2013

Early deformation history of the Yanshan Tectonic Belt is an unsolved, important issue. We report early structures and their dating results in basement rocks south of the Kalaqin metamorphic core complex. The basement deformation zone is characterized by WNW-ESE steep gneissosity, WNW-ESE shallow mineral elongation lineation and many intrafolial or isoclinal folds. Many kinematic indicators show that it is a WNW-ESE steep, ductile sinistral deformation zone. LA-ICPMS zircon dating gives a crystallization age of 271 Ma for tatolly transposed, deformed monzonite granite dyke and crystallization ages of 251–250 Ma and 210 Ma for undeformed dyke, stock and pluton. The dating results demonstrate that the deformation related to regional shortening took place between 271 and 251 Ma, i.e. Middle-Late Permian. Combined with previous dating results for post-orogenic magmatism in the Yanshan Tectonic Belt, it is inferred that the shortening-related deformation happened in Middle Permian (271–260 Ma). Recent studies suggest that collision along the Solonker Suture took place in Middle Permian, and is then followed by post-collision extenion in Late Permian. We propose that the intense shortening deformation of the Middle Permian in the Yanshan Tectonic Belt belongs to foreland deformation along the norterhn margin of the North China Craton which is caused by continent-continent collision in the Xing-Meng Orogen. The belt was then oriprinted by shortening deformation of the Yanshanian Movement.

Yanshan Tectonic Belt, foreland deformation, metamorphic basement, zircon U-Pb dating, dyke, Xing-Meng Orogen

Citation: Lin S Z, Zhu G, Yan L J, et al. Structural and chronological constraints on a Late Paleozoic shortening event in the Yanshan Tectonic Belt. Chin Sci Bull, 2013, 58: 3922–3936, doi: 10.1007/s11434-013-5926-8

The Xing-Meng Orogen, the eastern segment of the Central Asian Orogen, results from subduction and closure of the Paleo-Asian Ocean. Recent studies demonstrate that the Paleo-Asian Ocean subducted southwards underneath the North China Craton during Late Paleozoic [1–5]. Final collision of the Mongolian Block and North China Craton along the Solonker suture took place in Middle Permian [5–7]. Magmatism features suggest that the Yanshan Tectonic Belt (YTB), the northern margin of the North China Craton, was in a magmatic arc setting of active continental margin before Middle Permian [2,3,8–11], and in a post-orogenic extensional setting between Late Permian and Triassic [10–12].

Initial deformation time of the YTB related to the Xing-Meng Orogen is an unsolved and important issue. It is not clear if the YTB experiences Late Paleozoic deformation. On the basis of studies on the Pingquan-Gubeikou Fault, Davis et al. [13,14] suggested that the earliest deformation in the YTB, characterized by southward thrusting, happened before 180 Ma. However, accurate time of the deformation is unclear. Hu et al. [15] argued from ages of strata cut by the fault that the deformation took place in Early Triassic, and represent the earliest shortening in the cover. Zhao [16], Cui and Wu [17] also proposed that the earliest shortening deformation in the cover took place in the Indosinian event of Triassic. Hu et al. [18] reported biotite $^{40}Ar/^{39}Ar$ ages of 399 and 263 Ma from mylonites in the Shangyi-Chicheng Fault in the south of the YTB. However, Wang [19] obtained a hornblende $^{40}Ar/^{39}Ar$ age of 211 Ma from a mylonite sample in the same fault. Geological meaning of the different ages are unclear. In summary, early deformation

*Corresponding author (email: 502967277@qq.com)

history in the cover along the northern margin of the North China Craton remains controversial. This important and significant issue is related to understanding of origination and evolution of the YTB, destruction history of the North China Craton as well as tectonic evolution of the Xing-Meng Orogen.

The Kalaqin metamorphic core complex (KMCC) south of Chifeng, Inner Mongolia, lies at the northern margin of the YTB. Large-scale high-grade metamorphic basement rocks are exposed south of the Kalaqin batholith. Liu et al. [20] obtained a K-feldspar-plagioclase-whole-rock Rb-Sr isochron age of 232 Ma from a mylonite sample in the basement, and interpreted it as representing a deformation age. However, this interpretation needs to be further testified. After detailed structural investigation and zircon dating of dykes with different deformation history, this paper offers reliable constraints on an early deformation event in the YTB.

1 Geological setting

This study area lies south of the KMCC. The KMCC around Kalaqinqi, Chifeng, Inner Mongolia is situated in the north of the YTB at the northern margin of the North China Craton. The area neighbors the Xing-Meng Orogen to the north. The KMCC extends NE-SW in general and has a length of ca. 160 km and a width of 35 km. Its core complex is composed of high-grade metamorphic basement rocks and plutons of Late Paleozoic and Mesozoic. Cambrian and Permian cover strata are locally preserved above the core complex. Rift basins appear on the both sides of the KMCC (Figure 1).

Metamorphic basement rocks in the area are the Jianping Complex of Neoarchean to Paleo-proterozoic. The complex includes high-grade metamorphic supracrustal and igneous rocks such as plagioclase amphibolite, hornblende-plagioclase gneiss, biotite-plagioclase gneiss, which are dioritic or granitic gneisses belonging to TTG series with different degrees of migmatization. From LA-ICPMS zircon U-Pb dating and metamorphic researches for the basement complexes in the Jianping region east of this study area, Liu et al. [22] suggested that protolith ages of the high-grade rocks range from 2555 to 2550 Ma, and they experienced a TTG magmatism stage of 2538–2459 Ma, granulite-facies metamorphism stage of 2458 Ma and retrograde metamorphism stage of 2450–2401 Ma.

The Pingzhuang and Xiaoniu rift basins appear on the eastern and western side of the KMCC respectively (Figure 1). Exposed strata in the Pingzhuang Basin include volcanic rocks of the Yixian Formation (K_1y), Jingangshan Formation (K_1j), Tuhulu Formation (K_1t) and clastic rocks of the Jiufotang Formation (K_1jf), Binggou Formation (K_1b), Fuxin Formation (K_1f) and Sunjiawan Formation (K_1s) from bottom to top. The exposed strata in the Xiaoniu Basin are volcanic rocks of the Yixian Formation (K_1y), Jingangshan Formation (K_1j) and Tuhulu Formation (K_1t).

Many plutons appear in the core complex and their exposure area occupies ca, 60% of the exposed core complex (Figure 1). Previous zircon dating [13,21,23–26] yields ages of Late Paleozoic to Mesozoic for these plutons. The Late Paleozoic plutons are dominated by intermediate monzonite granite such as the Guodishan pluton (254 Ma [13], 253 Ma [21]), Nangoumen pluton (286 Ma [21]), Permian granite intrusions around Kalaqin and Meilin as well as Lamadong granite pluton of Early Carboniferous (327 Ma [23]). Mesozoic plutons, as main parts of the Kalaqin batholith, predominate in the core complex, and show NE-extension. Middle Triassic to Early Jurassic plutons in this area are diorite, quartz diorite, granodiorite or monzonite granite, such as the Ningcheng pluton (228–219 Ma [26]), Guangdingshan pluton (207 Ma [26], 204 Ma [21]) and Daxigoumen pluton (209 Ma, this study). Middle-Late Jurassic plutons are monzonite granite including the Maanshan pluton (156 Ma [25]) and Dajianshan pluton. Early Cretaceous plutons in the core complex are monzonite granite and granodiorite such as the NW-extending Anjiayingzi Pluton (132 Ma [24]).

The NNE-striking Louzidian-Dachengzi and Jinshan-Meilin ductile shear zones occur along the eastern and western margins of the KMCC (Figure 1). The shear zones show consistent top-to-the-NE sense of shear [27]. The KMCC is considered as being developed in Early Cretaceous from biotite $^{40}Ar/^{39}Ar$ ages of 126–133 Ma [28,29] for the Louzidian-Dachengzi shear zone and hornblende or biotite $^{40}Ar/^{39}Ar$ ages of 126–134 Ma [29] for the Jinshan-Meilin ductile shear zone. Metamorphic basement rocks in footwall of the KMCC experienced intense ductile deformation and show penetrative NE-SW foliation and mineral lineation. The footwall show similar fabrics and shear sense to those in the detachment ductile shear zones. The eastern shear zone and its footwall basement rocks show SE-dipping foliation whereas the western shear zone and its footwall basement rocks present NW-dipping foliation. They all show NE-trending mineral lineation and top-to-the-NE sense of shear. These indicate that the footwall basement rocks were widely involved in this phase of deformation [27]. Detachment normal faults were developed along the two ductile shear zones during exhumation of the KMCC [27,30], and show top-to-the-NW or SE sense of shear. It is noted that exposed basement rocks just south of the KMCC, i.e. from Sanshijiazi to Toudaoyingzi (Figure 1) lie in the hanging-wall of the detachment shear zone and show different fabrics from those in the footwall. These suggest that the basement rocks just south of the KMCC have not involved in the core complex deformation and can be used as understanding early deformation history in the YTB.

2 Deformation characteristics south of the KMCC

2.1 Basement deformation

Detailed investigation was conducted on deformation fabrics

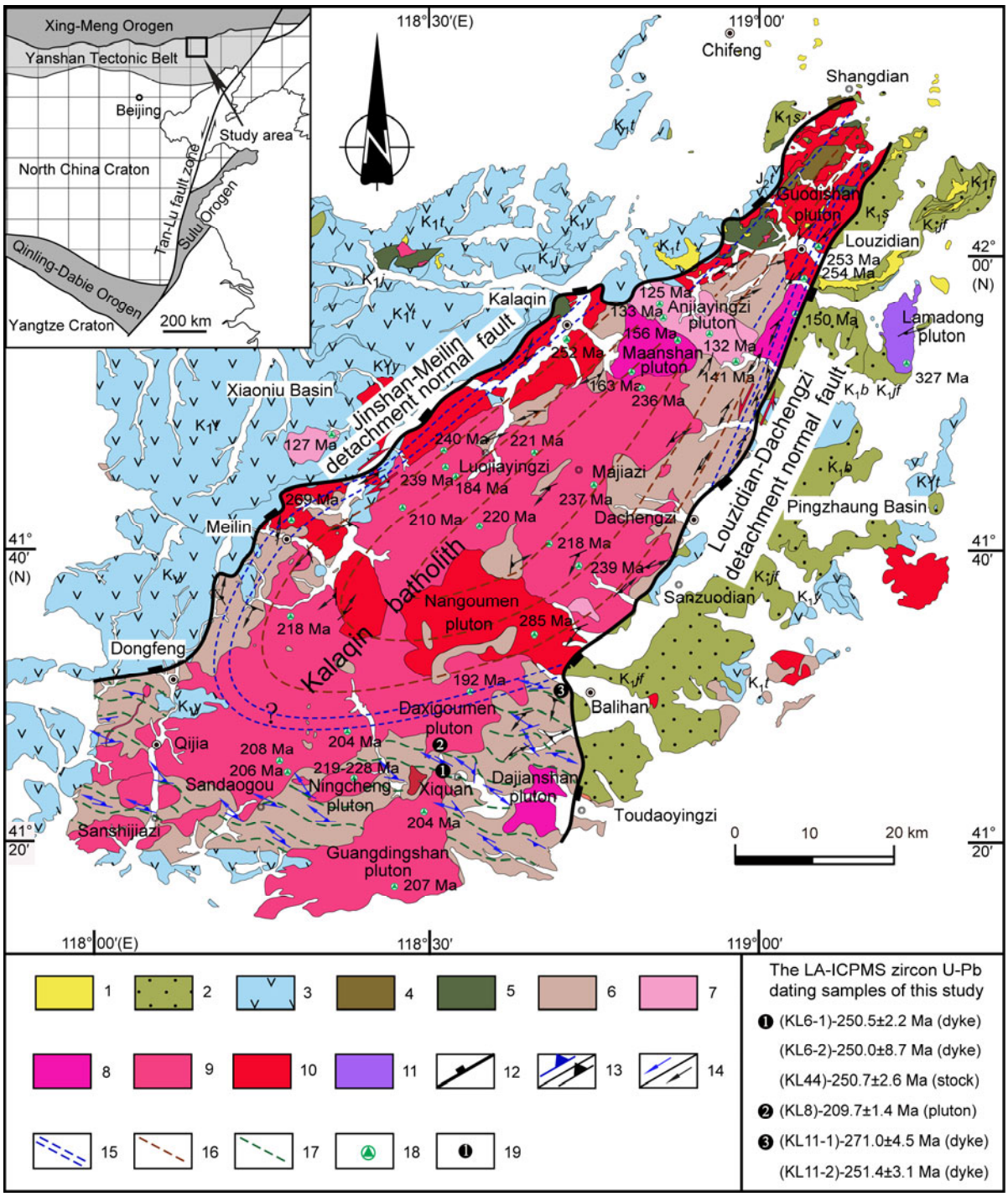

Figure 1 Structural map for the Kalaqin metamorphic core complex and its neighboring area (modified from 1∶200000 geological maps of Chifeng, Aohanqi, Weichang, Kalaqinqi, Jianping and Pingquan and after Wang et al. [21]). 1, Neogene; 2, Early Cretaceous terrestrial clastic rocks, including the Sunjiawan Foramtion (K_1s), Fuxin Formation (K_1f), Binggou Formation (K_1b) and Jiufotang Formation (K_1jf) from bottom to top; 3, Early Cretaceous volcanic rocks, including the Tuhulu Formation (K_1t), Jingangshan Formation (K_1j) and Yixian Formation (K_1y) from bottom to top; 4, Qingfengshan Formation of Permian; 5, Cambrian; 6, Jianping complex of Neoarchean to Paleo-proterozoic; 7, Early Cretaceous pluton (K_1); 8, Middle-Late Jurassic pluton; 9, Late Triassic to Early Jurassic pluton; 10, Permian pluton; 11, Early Carboniferous pluton; 12, brittle normal fault; 13, earlier/later foliation attitude; 14, earlier/later mineral elongation lineation attitude; 15, later ductile shear zone; 16, foliation trajectory in the MCC; 17, foliation trajectory in the southern basement; 18, previous dating sample locality (from Wang et al. [21]); 19, dating sample locality for this study.

in the basement rocks just south of the KMCC in this work. The metamorphic basement rocks in the area are dioritic to granitic gneisses such as plagioclase amphibolite, hornblende-plagioclase gneiss and biotite-plagioclase gneiss. Compositional layering in the metamorphic rocks is parallel to deformation foliation, and shows steep to nearly vertical

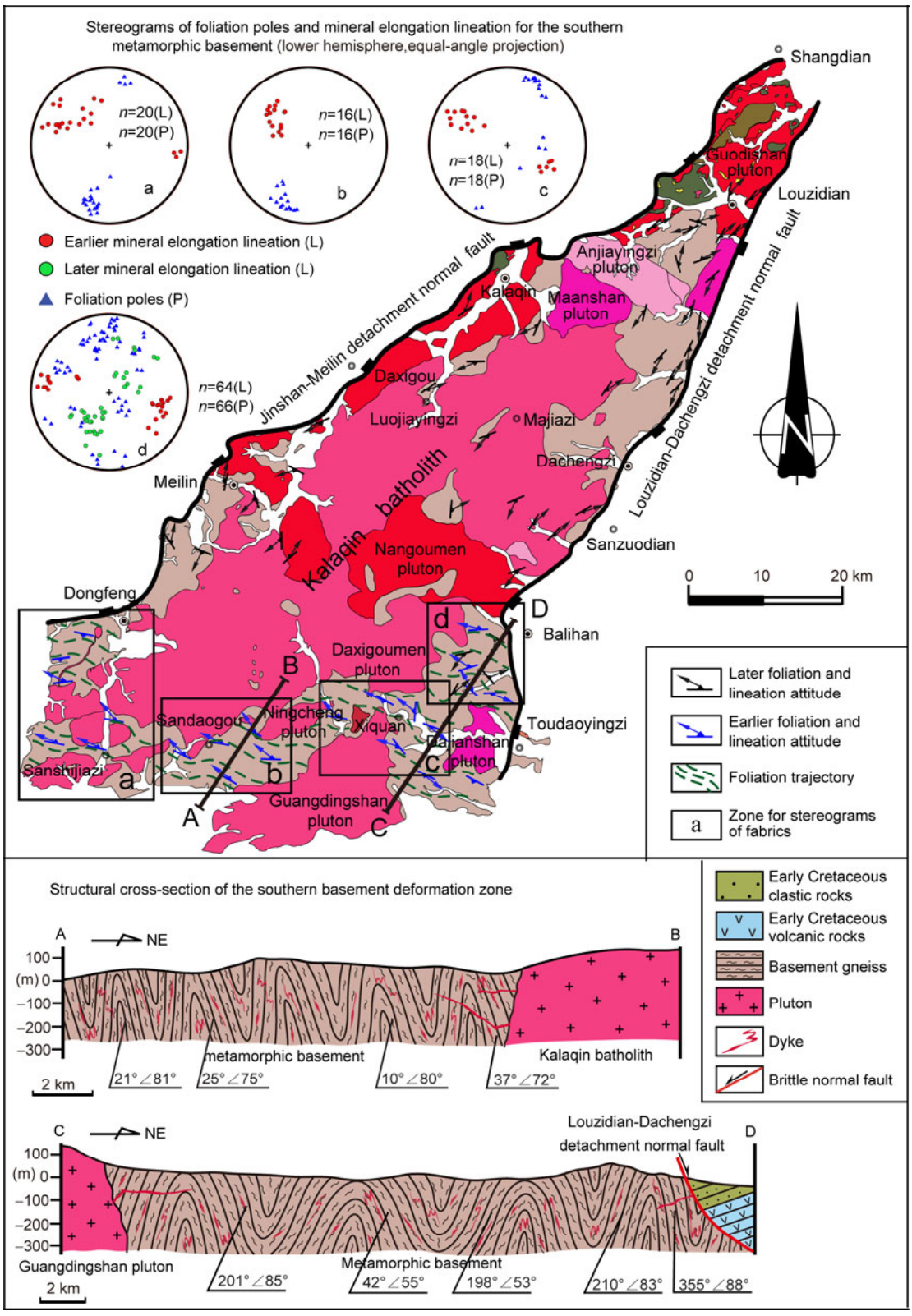

Figure 2 Stereograms of fabrics and structural cross-section for the metamorphic basement rocks south of the Kalaqin metamorphic core complex.

attitudes (Figure 3(a)).

Gneissosity in the western basement rocks, i.e. from Sanshijiazi to Sandaogou, strikes WNW-ESE, dips NNE mostly with dip angles of 70°–85°(Figure 2(a),(b)) whereas it strikes WNW-ESE, but dips SSW mostly (Figure 2(c)) in the eastern basement rocks around Xiquanxiang. It shows

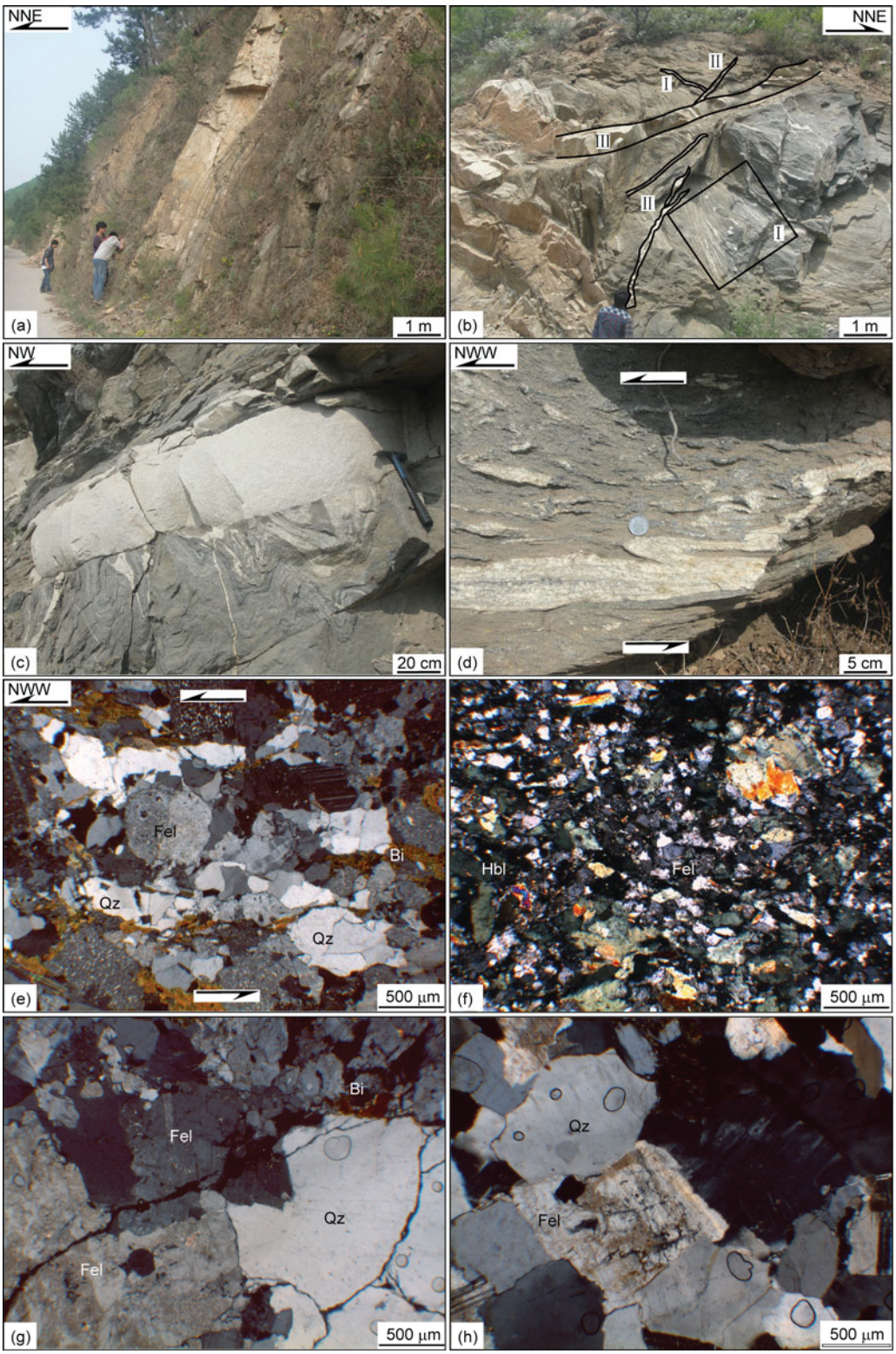

Figure 3 Outcrop photographs and photomicrographs for the southern basement deformation zone. (a) Steep foliation in the southern basement; (b) three-stage dykes in the basement, including earlier totally transposed dyke (I), middle-stage partially transposed dyke (II) and later undeformed dyke (III); (c) foliation in host gneiss is nearly perpendicular to boundary of an undeformed dyke; (d) folded granite dyke in the basement, indicating top-to-the-WNW sense of shear; (e) photomicrograph for a dated, earlier deformed dyke (KL11-1) in the basement, showing oriented arrangement of feldspar and biotite, oriented elongation of quartz and top-to-the-WNW sense of shear as indicated by oblique array of minerals; (f) photomicrograph for a dated, undeformed diabase dyke (KL11-2) with minerals of feldspar, hornblende and biotite; (g) photomicrograph for a dated, undeformed granite dyke (KL6-1), showing brittle fractures of feldspar and quartz, no mineral oriented arrangement and plastic elongation; (h) photomicrograph for the dated, undeformed Daxigoumen granite pluton (KL8), showing no mineral oriented arrangement and plastic elongation.

predominant E-W strikes with varied dip directions in the eastern basement rocks near the eastern detachment shear zone (Figure 2(d)), suggesting influence by the later KMCC deformation.

Mineral elongation lineation in the basement rocks far away from the detachment shear zone trends NW-SE and plunges shallowly NW in the west and NW or SE in the east. However, it shows varied attitudes with approaching the eastern detachment shear zone (Figure 2(d)), similar to the gneissosity. Lineation near the shear zone trends from WNW-ESE to NE-SW, shows varied plunging angles and shallower plunging angles for WNW-ESE one. It is suggested that varied attitudes of fabrics in the eastern basement rocks near the detachment shear zone are related to local transposition or reworking by the later extensional deformation of the KMCC, resulting in local preservation of early fabrics.

Our field investigation reveals that compositional layering in the metamorphic basement rocks are folded intensely. Inclined, isoclinal folds with NW-striking, NNE-dipping axial planes and shallow axes parallel to mineral lineation are common in the western basement (Figure 2). Steep, tight folds with NW-striking axial planes and axes parallel to mineral lineation predominate in the eastern basement (Figure 2). Small-scale intrafolial, rootless folds and shear folds are well developed in the basement rocks.

S-C fabrics, tails of feldspar porphyroclasts, asymmetrical small folds in the basement rocks with NW-trending mineral lineation show sinistral sense of shear. The shear indicators suggest top-to-the-NW sense of shear for N-dipping or NNE-dipping foliation (Figure 3(d)) while they indicate top-to-the-SE sense of shear for S-dipping or SSW-sipping foliation.

In summary, the southern basement rocks show different fabrics and kinematics from those inside of the KMCC. Only the eastern end of the southern basement rocks near the eastern detachment shear zone presents fabrics affected by the later extensional deformation of the KMCC. Early structures in the southern basement are characterized by tight, A-type folds (with fold axes parallel to lineation), WNW-striking, steep foliation, WNW-trending, shallow mineral lineation and sinistral shearing. It is suggested therefore that a steep strike-slip ductile deformation zone resulting from NE-SW shortening occurs in the southern basement. A large-scale mylonite belt has not been found in the southern basement in our field work, but small-scale mylonite belts with widths of several centimeters to tens of centimeters appear in local strain localization belts, i.e. NWW-striking small sinistral ductile shear belts.

2.2 Deformation of plutons and dykes

Field structures, microstructures and previous dating results demonstrate that plutons of Late Triassic to Late Jurassic around the southern basement have not been involved in ductile deformation. These plutons include the Ningcheng quartz diorite, pyroxene diorite pluton with LA-ICPMS zircon ages of 228–219 Ma [26], Guangdingshan granite pluton with LA-ICPMS zircon ages of 208–204 Ma [21,26], Daxigoumen monzonite granite pluton with a LA-ICPMS zircon age of 209.7±1.4 Ma (this study) and Dajianshan pluton of Middle-Late Jurassic ages [21].

Dykes in the southern basement deformation zone are dominated by granite, monzonite granite and diabase, and small stocks are mostly granite. The dykes can be classified into three types, i.e. totally transposed dykes, partially transposed dykes and undeformed dykes (Figure 3(b)). The earliest, totally transposed dykes show intense ductile deformation, similar penetrative foliation and lineation to their host basement rocks, common intrafolial folds and boudinages. Boundary planes of the totally transposed dykes is parallel or slightly oblique to the host basement foliation. The partially transposed dykes are syn-kinematic dykes emplaced during the deformation. Their boundary planes are oblique to the host basement foliation. Degrees of folding and boudinage in the partially transposed dykes are weaker than those in the totally transposed ones. Foliation related to ductile deformation also appears in the partially transposed dykes. They are good shear sense indicators that all suggests WNW-striking sinistral deformation in the involved rocks. The undeformed dykes show no plastic deformation and crosscut the host basement foliation with high angles (Figure 3(c)). They include coarse granite, pegmatite and diabase. Diabase dykes in the southern basement are undeformed. The three types of dykes can be used for timing deformation in the southern deformation zone.

3 Zircon U-Pb dating

3.1 Sample description

To date deformation in the basement south of the KMCC, one totally transposed dyke sample, three undeformed dyke samples, one undeformed small stock sample and one undeformed pluton sample were collected for LA-ICPMS zircon U-Pb dating. Partially transposed dykes in the area are too thin to collect for dating samples. Sampling localities are shown in Figure 1. Lithology, main features and dating results of the samples are listed in Table 1.

Samples KL11-1 and KL11-2 were collected from the eastern end of the southern basement deformation zone at one outcrop west of Balihan (Figure 4(a),(b)), and one is about 15 m distant from another. This basement outcrop has early NW-striking foliation and NW-trending mineral elongation lineation, showing no influence of the later core complex ductile deformation. The sample KL11-1 is totally transposed monzonite granite dyke with penetrative foliation and mineral lineation parallel to those in the host metamorphic rocks (Figure 4(a)). Microscopic observation shows oriented arrangement of feldspar and elongation of quartz

Table 1 Deformation features and dating results of the U-Pb zircon dating samples

Sample No.	Rock type	Mineral assemblage	Deformation phenomena	Intrusion stage	Age (Ma)
KL11-1	monzonite granite dyke	plagioclase+K-fekspar+quartz+biotite	intensely deformed	synkinematic or predating	271.0±4.5
KL11-2	diabase dyke	hornblende+biotite+plagioclase+pyroxene	undeformed	post-deformation	251.4±3.1
KL44	granite stock	plagioclase+quartz+biotite	undeformed	post-deformation	250.7±2.6
KL6-1	granite dyke	plagioclase+quartz+biotite	undeformed	post-deformation	250.5±2.2
KL6-2	diabase dyke	hornblende+biotite+plagioclase+pyroxene	undeformed	post-deformation	250.0±8.7
KL8	monzonite granite pluton	plagioclase+K-feldspar+quartz+biotite	undeformed	post-deformation	209.7±1.4

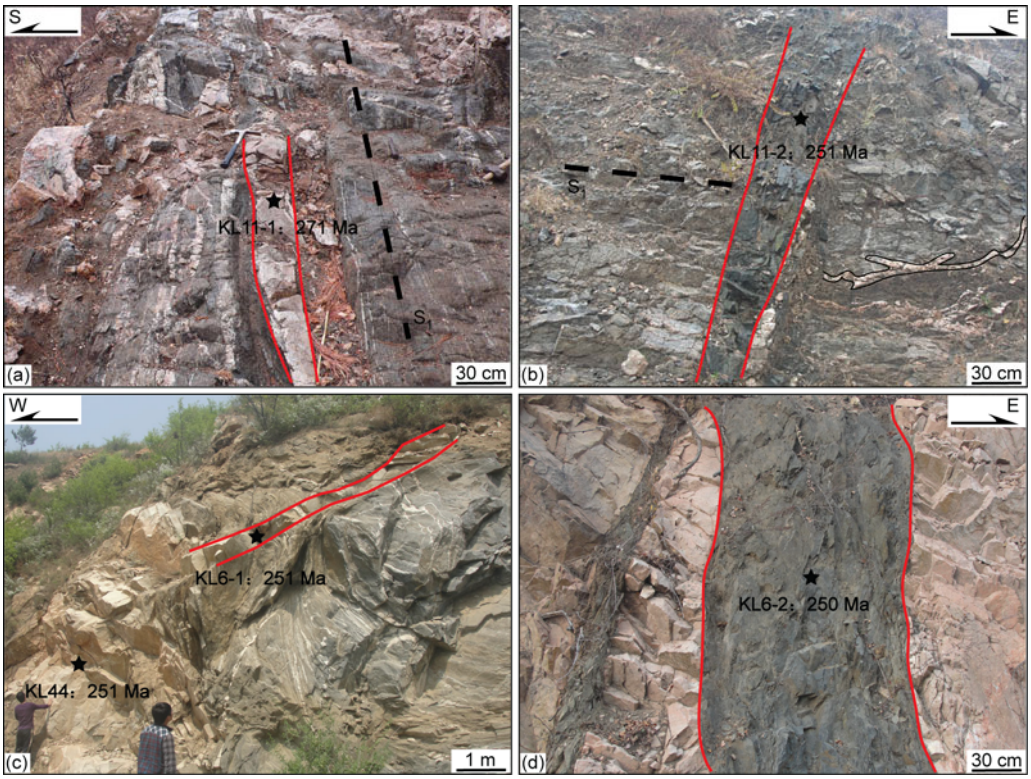

Figure 4 Outcrop photographs for the dated dykes.

for the sample, further proving its deformation (Figure 3(e)). The sample KL11-2 is undeformed diabase dyke with an attitude perpendicular to host basement foliation and cross-cutting earlier deformed granite dykes, suggesting being not involved in the basement ductile deformation (Figure 4(b)). Microscopic observation further confirms no ductile deformation of the sample (Figure 3(f)).

Samples KL44, KL6-1, KL6-2 are undeformed samples from the same outcrop in the eastern basement south of the KMCC and west of Xiquan. Sample KL44 is a undeformed, fine-grained small granite stock (Figure 4(c)). Sample KL6-1 is a branch dyke from the KL44 stock (Figure 4(c)). Sample KL6-2 is a diabase dyke intruding an undeformed stock just west of the above two samples (Figure 4(d)). Although the diabase dyke was not involved in ductile deformation of the host basement, it experienced later brittle sliding along the dyke boundary planes and was cleavaged (Figure 4(d)). Microscopic observation further confirms no plastic deformation in the three samples (Figure 3(g)).

Sample KL8 is from the Daxigoumen coarse, porphyritic monzonite granite pluton southeast of the KMCC. Field and microscopic investigation demonstrate that it is a undeformed pluton intruding after the host basement deformation.

3.2 Sample preparation and analytical methods

Zircon grains from the dated samples were separated using conventional heavy liquid and magnetic techniques. Representative zircon grains were handpicked under a binocular microscope and mounted in an epoxy resin disc, and then analyzed for Cathodoluminescence (CL) images of zircon grains and U-Pb isotopes at the State Key Laboratory of Geological Processes and Mineral Resources, China University

of Geosciences, Wuhan. Laser ablation ICP-MS (LA-ICP-MS) U-Pb analyses of the magmatic zircon grains were conducted on an Agilent 7500a ICP-MS equipped with 193 nm Geo-Las2005 Laser. Zircon 91500 was used as an external standard. The external standard silicate glass NIST SRM 610 and internal standard ^{29}Si were used to correct element contents. The detailed analytical technique and machine data is described by reference [31]. Zircon U-Pb age calculations were made by using an program described by reference [32]. Common Pb correction was made by using the Andersen method [33]. Concordia diagrams and weighted mean calculations were made by using an Isoplot 3.0 Program.

3.3 Dating results

U-Pb isotope data of the dated samples are listed in Table 2. Cathodoluminescence images of the dated zircon are shown

Table 2 Zircon U-Pb dating results

Spot No.	Th (μg/g)	U (μg/g)	Th/U	$n(^{207}Pb/^{206}Pb)$		$n(^{207}Pb/^{235}U)$		$n(^{206}Pb/^{238}U)$		$^{207}Pb/^{235}U$ Age (Ma)	$^{206}Pb/^{238}U$ Age (Ma)
				Ratio	Error (1σ)	Ratio	Error (1σ)	Ratio	Error (1σ)		
Sample KL11-1 (118°41′54″E, 41°31′02″N)											
1	232	623	0.37	0.05158	0.00211	0.30369	0.01209	0.04265	0.00056	269±9	269±3
2	155	478	0.32	0.05121	0.00221	0.30286	0.01282	0.04275	0.00057	269±10	270±4
3	30	220	0.14	0.05148	0.00343	0.30523	0.01951	0.04343	0.00067	270±15	274±4
4	161	489	0.33	0.05107	0.00211	0.30636	0.01298	0.04314	0.00050	271±10	272±3
Sample KL11-2 (118°41′54″E, 41°31′02″N)											
1	417	1972	0.21	0.05843	0.00235	0.31821	0.01201	0.03950	0.00054	281±9	250±3
2	115	1202	0.10	0.05033	0.00169	0.27518	0.00877	0.03966	0.00043	247±7	251±3
3	477	1954	0.24	0.06396	0.00247	0.34853	0.01231	0.03952	0.00062	304±9	250±4
4	340	1370	0.25	0.05121	0.00190	0.28772	0.01052	0.04034	0.00051	257±8	255±3
5	206	2530	0.08	0.05285	0.00147	0.29252	0.00781	0.03973	0.00038	261±6	251±2
Sample KL44 (118°30′28″E, 41°25′33″N)											
1	204	470	0.43	0.05347	0.00349	0.29115	0.01845	0.03949	0.0006	259±15	250±4
2	265	260	1.02	0.05508	0.00386	0.29331	0.01841	0.03967	0.0007	261±14	251±4
3	167	233	0.72	0.05339	0.00330	0.28730	0.01722	0.03976	0.0007	256±14	251±4
4	276	292	0.95	0.05982	0.00312	0.32902	0.01751	0.03986	0.0006	289±13	252±4
5	200	313	0.64	0.06133	0.00362	0.33355	0.02083	0.03914	0.0006	292±16	248±4
6	94	134	0.70	0.06016	0.00415	0.33146	0.02356	0.04005	0.0008	291±18	253±5
7	151	188	0.81	0.05871	0.00363	0.32068	0.01971	0.03996	0.0008	282±15	253±5
8	190	205	0.92	0.06060	0.00434	0.33388	0.02498	0.03965	0.0007	293±19	251±4
9	309	349	0.89	0.05579	0.00313	0.30310	0.01634	0.03987	0.0006	269±13	252±3
10	146	189	0.77	0.05574	0.00459	0.30615	0.02399	0.04037	0.0008	271±19	255±5
11	299	385	0.78	0.05497	0.00295	0.30006	0.01538	0.03991	0.0005	266±12	252±3
12	311	472	0.66	0.05536	0.00267	0.29928	0.01439	0.03884	0.0005	266±11	246±3
13	210	266	0.79	0.05466	0.00365	0.30187	0.02061	0.03970	0.0006	268±16	251±4
Sample KL6-1 (118°30′52″E, 41°25′38″N)											
1	52	72	0.73	0.06086	0.00923	0.33507	0.04995	0.03993	0.00111	293±38	252±7
2	580	995	0.58	0.05200	0.00187	0.28646	0.01037	0.03956	0.00045	256±8	250±3
3	1134	2373	0.48	0.05110	0.00158	0.27975	0.00872	0.03926	0.00038	250±7	248±2
4	248	431	0.58	0.05446	0.00289	0.30022	0.01667	0.03970	0.00062	267±13	251±4
5	224	372	0.60	0.04605	0.00228	0.25165	0.01211	0.03965	0.00049	228±10	251±3
6	1479	3005	0.49	0.05303	0.00143	0.29280	0.00814	0.03965	0.00044	261±6	251±3
7	264	690	0.48	0.05033	0.00262	0.27895	0.01391	0.04012	0.00063	250±11	254±4
8	243	946	0.26	0.04989	0.00227	0.27735	0.01260	0.04001	0.00057	249±10	253±4
9	251	248	1.01	0.05327	0.00285	0.29001	0.01529	0.03954	0.00064	259±12	250±4
10	1056	1719	0.61	0.04738	0.00125	0.26153	0.00668	0.03963	0.00039	236±5	251±2
11	1409	469	3.01	0.05161	0.00214	0.28426	0.01145	0.03975	0.00051	254±9	251±3
12	154	196	0.79	0.05781	0.00362	0.31112	0.01907	0.03963	0.00071	275±15	251±4

(*To be continued on the next page*)

(*Continued*)

Spot No.	Th (μg/g)	U (μg/g)	Th/U	$n(^{207}Pb/^{206}Pb)$		$n(^{207}Pb/^{235}U)$		$n(^{206}Pb/^{238}U)$		$^{207}Pb/^{235}U$ Age (Ma)	$^{206}Pb/^{238}U$ Age (Ma)
				Ratio	Error (1σ)	Ratio	Error (1σ)	Ratio	Error (1σ)		
Sample KL6-2 (118°30′52″E, 41°25′38″N)											
1	75	115	0.65	0.05192	0.00505	0.28199	0.02671	0.03939	0.00088	252±21	249±5
2	102	186	0.55	0.05485	0.00431	0.28785	0.02013	0.03970	0.00084	257±16	251±5
3	60	225	0.27	0.05302	0.00344	0.34006	0.02267	0.04596	0.00076	297±17	290±5
4	59	269	0.22	0.05087	0.00250	0.32199	0.01555	0.04608	0.00062	283±12	290±4
5	189	318	0.59	0.04887	0.00275	0.31997	0.01849	0.04652	0.00076	282±14	293±5
6	140	500	0.28	0.05167	0.00220	0.33622	0.01394	0.04689	0.00072	294±11	295±4
7	268	757	0.35	0.05298	0.00182	0.34160	0.01199	0.04616	0.00064	298±9	291±4
8	319	674	0.47	0.05228	0.00194	0.33630	0.01278	0.04611	0.00061	294±10	291±4
9	272	365	0.74	0.05535	0.00284	0.35689	0.01746	0.04647	0.00069	310±13	293±4
10	455	885	0.51	0.05186	0.00192	0.33262	0.01169	0.04616	0.00048	292±9	291±3
11	335	565	0.59	0.05553	0.00266	0.35116	0.01707	0.04540	0.00067	306±13	286±4
12	835	1357	0.61	0.05252	0.00174	0.33760	0.01104	0.04608	0.00050	295±8	290±3
13	481	323	1.49	0.06197	0.00293	0.39461	0.01827	0.04601	0.00065	338±13	290±4
14	721	928	0.78	0.05459	0.00187	0.35134	0.01195	0.04609	0.00052	306±9	290±3
15	356	516	0.69	0.05544	0.00228	0.35349	0.01422	0.04613	0.00068	307±11	291±4
16	1108	1904	0.58	0.05327	0.00153	0.33760	0.00926	0.04526	0.00042	295±7	285±3
17	347	441	0.79	0.05454	0.00261	0.35120	0.01713	0.04608	0.00066	306±13	290±4
18	290	1686	0.17	0.05461	0.00175	0.35501	0.01128	0.04684	0.00070	308±8	295±4
19	78	183	0.42	0.05369	0.00400	0.33875	0.02445	0.04576	0.00085	296±19	288±5
20	389	601	0.64	0.05365	0.00244	0.33860	0.01526	0.04545	0.00059	296±12	287±4
21	479	850	0.56	0.05102	0.00197	0.32600	0.01180	0.04609	0.00052	287±9	290±3
22	504	757	0.67	0.04619	0.00173	0.29619	0.01116	0.04604	0.00060	263±9	290±4
Sample KL8 (118°30′52″E, 41°26′50″N)											
1	270	408	0.66	0.05215	0.00261	0.23793	0.01150	0.03311	0.00043	217±9	210±3
2	214	279	0.77	0.05570	0.00344	0.25130	0.01497	0.03320	0.00044	228±12	211±3
3	449	425	1.05	0.05566	0.00269	0.25227	0.01169	0.03310	0.00045	228±9	210±3
4	189	289	0.65	0.05314	0.00273	0.24609	0.01295	0.03373	0.00050	223±11	214±3
5	434	403	1.08	0.05730	0.00278	0.25925	0.01208	0.03306	0.00051	234±10	210±3
6	161	270	0.60	0.05196	0.00309	0.23423	0.01378	0.03316	0.00051	214±11	210±3
7	264	249	1.06	0.05530	0.00258	0.25088	0.01132	0.03315	0.00046	227±9	210±3
8	224	269	0.83	0.05343	0.00343	0.24627	0.01699	0.03305	0.00049	224±14	210±3
9	240	312	0.77	0.04048	0.00320	0.18184	0.01404	0.03299	0.00047	170±12	209±3
10	263	353	0.75	0.04843	0.00250	0.22262	0.01192	0.03313	0.00052	204±10	210±3
11	606	374	1.62	0.06554	0.00640	0.29088	0.02803	0.03219	0.00052	259±22	204±3
12	210	269	0.78	0.04975	0.00480	0.22834	0.02167	0.03329	0.00058	209±18	211±4
13	264	278	0.95	0.06092	0.00608	0.27486	0.02692	0.03272	0.00062	247±21	208±4
14	325	427	0.76	0.06664	0.00731	0.31318	0.04149	0.03289	0.00050	277±32	209±3
15	424	439	0.97	0.05224	0.00231	0.23859	0.01063	0.03304	0.00044	217±9	210±3
16	401	407	0.98	0.04817	0.00269	0.21981	0.01187	0.03324	0.00053	202±10	211±3
17	285	488	0.58	0.05526	0.00341	0.25319	0.01584	0.03304	0.00052	229±13	210±3
18	229	272	0.84	0.04605	0.00235	0.21059	0.01022	0.03317	0.00053	194±9	210±3
19	228	275	0.83	0.05743	0.00377	0.25748	0.01543	0.03298	0.00052	233±12	209±3
20	102	212	0.48	0.05581	0.00339	0.25477	0.01615	0.03294	0.00053	230±13	209±3
21	118	101	1.17	0.06338	0.00497	0.28065	0.02182	0.03318	0.00084	251±17	210±5

in Figure 5, U-Pb concordia diagrams of the samples are present in Figure 6 and their zircon age spectra are shown in Figure 7.

Analyzed zircon from sample KL11-1 of deformed dyke has long-column shapes, and their CL images show a core-mantle structure mostly. The mantle has fan-shaped zoning or oscillatory zoning, and their Th/U ratios range from 0.32 to 0.37, with an exception giving a ratio value of 0.14. It is suggested therefore that 26 analytical zircon crystals are of magmatic origin. Four of the analytical zircon crystals for the magmatic mantle lie around the U-Pb concordia line, and their $^{206}Pb/^{238}U$ weighted mean age is 271.2±4.4 Ma. This age is interpreted as representing crystallization age of the deformed dyke.

Analyzed zircon from sample KL11-2, an undeformed diabase dyke, also shows long-column crystals, and their CL images exhibit a core-mantle structure mostly with a inherited magmatic core and oscillatory zoning mantle. Ratios of Th/U for 29 analyses on the mantle are greater than 0.1 with an exception yielding a Th/U ratio value of 0.08 due to higher U contents. Five of the magmatic zircon lie around the concordia line and give a $^{206}Pb/^{238}U$ weighted mean age of 251.4±3.1 Ma, representing a crystallization age.

Analyzed zircon from sample KL44 of undeformed stock shows long-column crystals, and their CL images indicate origin of magmatism. Ratios of Th/U from analyzed sites with oscillatory zoning range from 0.43 to 1.02, suggesting origin of magmatism. Thirteen of 30 analyses lie around the concordia line and give a weighted mean $^{206}Pb/^{238}U$ age of 250.7±2.6 Ma that is interpreted as representing an intrusion age.

Analyzed zircon from sample KL6-1 of undeformed dyke exhibits long-column crystals with CL images showing oscillatory zoning. Their Th/U ratios are between 0.48 and 3.01, indicating magmatic origin. Twelve of 30 analyses lie around the concordia line and give a weighted mean $^{206}Pb/^{238}U$ age of 250.5±2.2 Ma that is interpreted as a emplacement age of the dated dyke.

Analyzed zircon from sample KL6-2 of undeformed diabase dyke shows long-column crystals with CL images showing two types of zircon. One has a core with oscillatory zoning yielding Th/U ratios of 0.17–1.49 and white growing edge whereas another type shows magmatic mantle with oscillatory zoning giving Th/U ratios of 0.55–0.65. Twenty of 28 analyses on the core give a weighted mean $^{206}Pb/^{238}U$ age of 290.6±2.4 Ma that is interpreted as representing age of inherited zircon while other two analyses on the magmatic mantle yield a weighted mean $^{206}Pb/^{238}U$ age of 250.0± 8.7 Ma that is interpreted as representing an crystallization age of the dated diabase dyke. Although its crystallization age is only yielded from two analyzed zircon, another undeformed diabase sample (KL11-2) form the same outcrop also give the same crystallization age, suggesting reliability of the dating result for the sample KL6-2.

Analyzed zircon from sample KL8 of undeformed pluton show subhedral, long-column crystals with CL images showing oscillatory zoning of magmatic zircon. Ratios of Th/U for analyzed zircon of magmatic origin range from

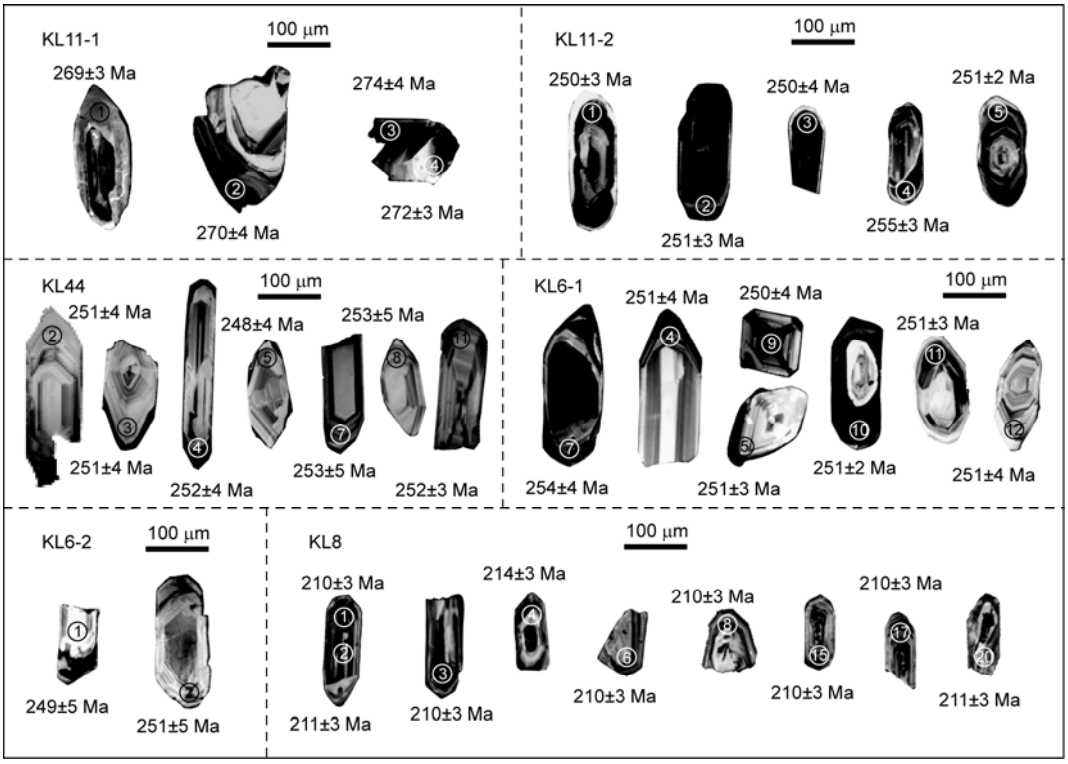

Figure 5 Zircon cathodoluminescence images with analytical sites and ages.

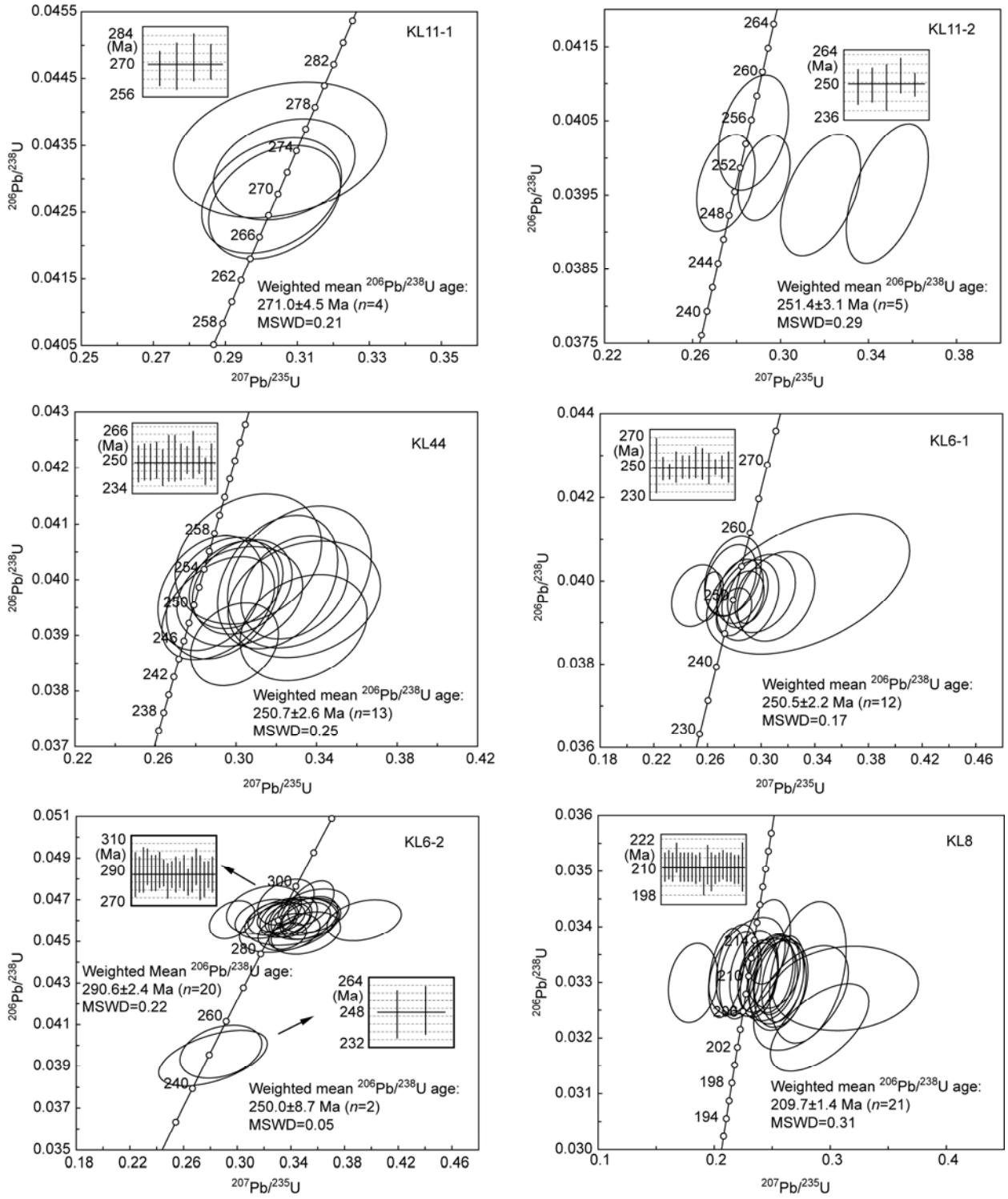

Figure 6 Zircon U-Pb concordia diagrams.

0.48 to 1.62. Twenty-one of 30 analyses lie around the concordia line and give a weighted mean $^{206}Pb/^{238}U$ age of 209.7±1.4 Ma that is interpreted as an intrusion age.

Frequentness statistics for all of the obtained zircon ages in this study show 5 age peaks (Figure 7), i.e. ca. 370 Ma (Late Devonian), ca. 290 Ma (Early Permian), ca. 270 Ma (Middle Permian), ca. 250 Ma (end of Late Permian) and ca. 210 Ma (Late Triassic). Their Th/U ratios (Table 2) suggest that the dated zircon is dominated by magmatic one, indicating 5 magmatic events in this area. These magmatic events are consistent with those recognized in the YTB [10] and KMCC, demonstrating reliability of our dating results.

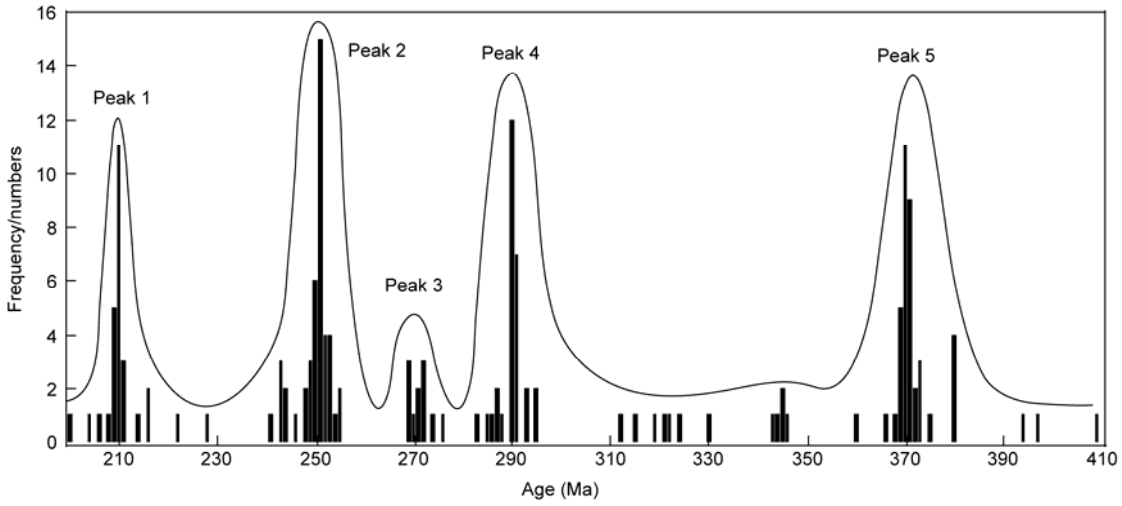

Figure 7 Zircon age spectra.

The Nangoumen and Meilin plutons have zircon ages of 285 and 269 Ma respectively (Figure 1) [21]. We also obtain LA-ICPMS zircon ages of 270.6±1.8 and 270.4±1.7 Ma for granite and monzonite granite in the Guodishan composite plutons in the north of the KMCC (to be published elsewhere). The above dating results further confirm reliability of the 271 Ma magmatic event in the southern basement deformation zone. Zircon ages of 253 [21] and 254 Ma [13] from plutons in the north of the KMCC have been reported previously. Zhang [26] also obtained a zircon age of 253 Ma from a diorite pluton in the KMCC. It is suggested therefore that the 250 Ma magmatic event also occurred north of our dating area. Previous dating results also show 210 Ma and younger magmatic events in the KMCC (Figure 1).

4 Interpretation of dating results

Six crystallization ages of dyke and pluton samples from the basement deformation zone south of the KMCC were obtained by means of the LA-ICPMS zircon U-Pb method. The totally transposed dyke (KL11-1) west of Balihan gives a crystallization age of 271 Ma, suggesting that the deformation took place at or after 271 Ma. The undeformed diabase dyke (KL11-2) near the sample KL11-1 yields a intrusion age of 250 Ma, indicating that the deformation happened before 250 Ma. The dating results for deformed and undeformed dykes from the same outcrop constrain the deformation between 271 and 250 Ma.

An undeformed small granite stock sample (KL44), granite dyke sample (KL6-1) and diabase dyke sample (KL6-2) from another outcrop in the southern basement deformation zone west of Xiquan give intrusion ages of 251, 251 and 250 Ma respectively. They are consistent within errors. The dating results of the three undeformed samples further confirm that the deformation took place before 250 Ma, and constrain it before 251 Ma actually.

The Kalaqin batholith north of the southern basement deformation zone was not involved in the ductile deformation. The Daxigoumen pluton northwest of Xiquan, the southeastern part of the batholith, gives a crystallization age of 210 Ma. The southern margin of the batholith, including the Ningcheng and Guangdingshan plutons, have zircon ages of 228–204 Ma [21,26]. It is demonstrated therefore that Late Triassic plutons were not involved in the ductile deformation of the southern basement, and the deformation happened before the Late Triassic.

In summary, our structural investigation and zircon dating results for dykes and plutons constrain the ductile deformation preserved in the basement south of the KMCC between 271 and 251 Ma, i.e. Middle-Late Permian. It is understood that the K-feldspar-plagioclase-whole-rock Rb-Sr isochron age from the southern basement mylonite, as reported by Liu et al. [20], cannot represent a deformation age for this area.

After chronological, petrological and geochemical studies for the Shijianfang pluton at the northern margin of the YTB at Faku, northern Liaoning Province, Zhang et al. [12] proposed that the YTB was involved in post-orogenic extension since 260 Ma. It is inferred from this result that the early shortening deformation in the YTB should take place in the Middle Permian of 271–260 Ma.

5 Tectonic property and dynamic setting for the Middle Permian deformation

5.1 Tectonic property

The basement deformation zone south of the KMCC is a WNW-ESE steep strike-slip ductile deformation zone. It is inferred from the ductile deformation that NE-SW shortening is responsible for its formation. This suggests that the NE-SW shortening took place in the study area during the

Middle Permian. The ductile deformation demonstrates that the exposed basement rocks were buried at ductile levels, i.e. more than 10 km deep, during the Middle Permian, and later uplifting led to its exposure to the surface. Penetrative fabrics and tight folds, mostly intrafolial, isoclinal folds, for the ductile deformation in the southern basement rocks indicate intense shortening during the Middle Permian. It is demonstrated therefore that the early deformation after deposition of marine cover in the YTB took place in the Middle Permian, rather than the Indosinian event as proposed by some authors previously [13–17].

It is well known that shortening structures, such as thrusts and folds, in the YTB strike WNW-ESE mostly [34]. They were superimposed by NE-trending, shortening structures, especially in its eastern segment [34]. The Yanshan Movement, shortening event, in the YTB just before and after Middle Jurassic has been widely accepted [13,14,35–38]. Considering later overprinting and local difference, the basement deformation structures south of the KMCC are congruous with regional WNW-striking shortening structures in general. It is inferred that the strike-slip structures recognized in the southern basement resulted from regional shortening, and are synchronous with the general WNW-striking shortening structures. Another possibility is that WNW-striking, strike-slip structures were widely developed in the YTB in the Middle Permian. However, this type of structures were seldom reported. We propose that the general WNW-striking shortening structures are products of this deformation. More detailed researches are needed to testify this interference.

Considering tectonic evolution of both the YTB and Xing-Meng Orogen in the north (seeing details later), we propose that the shortening deformation of the Middle Permian along the northern margin of the North China Craton belongs to foreland deformation. Its resultant structures striking WNW in general are foreland folds and thrusts. Previous detailed studies on Late Paleozoic igneous rocks demonstrated that the YTB of Late Paleozoic was in a magmatic arc setting of active continental margin before Middle Permian [2,3,8–11], post-collisional, extensional setting in Late Permian [12] or from the end of Late Permian [10,11] to Triassic. These results also support a foreland shortening stage of Middle Permian in the YTB. Disappearance history of the marine cover in the North China Craton shows deposition changes from paralic sediments of the Lower Permian Shanxi Formation, shallow marine to lake coal-bearing sediments of the Middle Permian Shang-Xia Shihezi Formations to terrestrial clastic sediments of the Upper Permian Shiqianfeng Formation, and indicates synchroneity of the marine cover disappearance and foreland deformation occurrence. The similar phenomena also appear in the Yangzte Plate where the Middle Triassic continent-continent collision [39–41] along the Qinling-Dabie-Sulu Orogen resulted in disappearance of marine cover in the Middle Triassic [42] and appearance of foreland terrestrial clastic rocks in Late Triassic [42,43]. In summary, we propose that the YTB originated from foreland deformation of the Middle Permian, and was then overprinted by the Yanshanian deformation in Jurassic.

5.2 Dynamic setting

Intense deformation and magmatism of Late Paleozoic in the eastern North China Craton only occur along its northern margin, the YTB. This reflects that its dynamics comes from the Xing-Meng Orogen in the north. On the basis of detailed chronological studies, Jian et al. [7] demonstrated that the collision in the Xing-Meng Orogen took place between 271 and 260 Ma. Li et al. [6] proposed from comprehensive analyses that the collision happened in Middle Permian (ca. 270 Ma). It is suggested therefore that the collision of the Mongolian Block and North China Craton and shortening deformation of Late Palaeozoic in the YTB took place at the same time, and the Middle Permian deformation in the YTB resulted from periphery foreland deformation caused by the collision of the Xing-Meng Orogen. Recognition of the Middle Permian foreland deformation in the YTB by this study also testify the Middle Permian final closure of the eastern Paleo-Asian Ocean as suggested previously.

Many studies in the Xing-Meng Orogen [7,10,11,44,45] demonstrated that the orogen switched into a post-orogenic extensional setting characterized by the wide appearance of alkaline or A-type granite and a swarm of diabase dykes. This post-orogenic extensional magmatism also affected the YTB as early as 260 Ma [12]. The magmatic events of 251, 250 and 210 Ma in the YTB recognized by this study should result from the influence of the post-orogenic extension in the Xing-Meng Orogen.

In summary, the collision of the Xing-Meng Orogen along the Solonker Suture and followed post-orogenic extension are synchronous with the foreland deformation and magmatism under an extension setting in the YTB respectively. This suggests that tectonic evolution at the northern margin of the North China Craton during Late Paleozoic to Triassic is controlled by the Xing-Meng Orogen in the North, and the latter can account for intense tectonic and magmatic events of Late Paleozoic in the YTB.

6 Conclusions

(1) Earlier ductile fabrics are preserved in the basement metamorphic rocks south of the KMCC, indicating no deformation overprinting by the later ductile deformation of the MCC. The basement deformation zone is characterized by WNW-striking steep foliation, WNW-trending shallow mineral lineation and intrafolial or isoclinal folds. Many kinematic indicators demonstrate that the deformation zone is a sinistral ductile zone produced by regional shortening.

(2) The totally transposed monzonite granite dyke in the basement gives a crystallization age of 271 Ma while the undeformed dykes, stock and pluton yield crystallization ages of 251–250 and 210 Ma respectively. These dating results constrain the basement ductile deformation between 271 and 251 Ma, i.e. Middle-Late Permian. Considering previous dating results for post-orogenic extensional plutons in the YTB, it is inferred that the shortening deformation in the YTB took place during a period of 271–260 Ma (Middle Permian).

(3) Our dating results demonstrate that the early shortening deformation in the YTB happened in the Middle Permian. The general WNW-striking shortening structures in the YTB should result from this phase of deformation that was followed by overprinting of the Yanshanian Movement. Comparison with recent studies for the Xing-Meng Orogen suggests that the Middle Permian shortening deformation of the YTB results from foreland deformation along the northern margin of the North China Craton that was caused by final closure of the Solonker Suture.

We gratefully acknowledge helps for zircon dating from Hu Zhaochu and Zheng Shu at the State Key Laboratory of Geological Processes and Mineral Resources, China University of Geosciences, Wuhan. Zhao Tian from Hefei University of Technology participated in some of the fieldwork. We give our sincerest thanks to Meng Qinren and Dong Yunpeng for their constructive comments that improved the final version of the manuscript. This work was supported by the National Natural Science Foundation of China (91214301).

1 Yin A, Nie S Y. A Phanerozoic palinspastic reconstruction of China and its neighboring regions. In: Yin A, Harrison T M, eds. The Tectonic Evolution of Asia. New York: Cambridge University Press, 1996. 442–485
2 Xiao W J, Windley B F, Hao J, et al. Accretion leading to collision and the Permian Solonker suture, Inner Mongolia, China: Termination of the central Asian orogenic belt. Tectonics, 2003, 22: 1069–1076
3 Zhang S H, Zhao Y, Song B, et al. Carboniferous granitic plutons from the northern margin of the North China block: Implications for a late Paleozoic active continental margin. J Geol Soc Lond, 2007, 164: 451–463
4 Zhang S H, Zhao Y, Song B, et al. Contrasting Late Carboniferous and Late Permian-Middle Triassic intrusive suites from the northern margin of the North China craton: Geochronology, petrogenesis, and tectonic implications. Geol Soc Am Bull, 2009, 121: 181–200
5 Zhang S H, Zhao Y, Kröner A, et al. Early Permian plutons from the northern North China Block: Constraints on continental arc evolution and convergent margin magmatism related to the Central Asian Orogenic Belt. Int J Earth Sci, 2009, 98: 1441–1467
6 Li J Y, Gao L M, Sun G H, et al. Shuangjingzi middle Triassic syncollisional crust-derived granite in the east Inner Mongolia and its constraint on the timing of collision between Siberian and Sino-Korean paleo-plates (in Chinese). Acta Petrol Sin, 2007, 23: 565–582
7 Jian P, Liu D Y, Kroner A, et al. Evolution of a Permian intraoceanic arc-trench system in the Solonker suture zone, Central Asian Orogenic Belt, China and Mongolia. Lithos, 2010, 118: 169–190
8 Zhang S H, Zhao Y, Song B. Hornblende thermobarometry of the Carboniferous granitoids from the Inner Mongolia Paleo-uplift: Implications for the geotectonic evolution of the northern margin of North China block. Mineral Petrol, 2006, 87: 123–141
9 Wang H C, Zhao F Q, Li H M, et al. Ziron SHRIMP U-Pb age of the dioritic rocks from northern Hebei: The geological records of late Paleozoic magmatic arc (in Chinese). Acta Petrol Sin, 2007, 23: 597–604
10 Zhang S H, Zhao Y, Liu J M, et al. Geochronology, geochemistry and tectonic setting of the Late Paleozoic-Early Mesozoic magmatism in the northern margin of the North China Block: A preliminary review (in Chinese). Acta Petrol Et Mineral, 2010, 29: 824–842
11 Zhao Y, Chen B, Zhang S H, et al. Pre-Yanshanian geological events in the northern margin of the North China Craton and its adjacent areas (in Chinese). Geol Chin, 2010, 37: 900–915
12 Zhang X H, Zhang H F, Wilde S A. Late Permian to Early Triassic mafic to felsic intrusive rocks from North Liaoning, North China: Petrogenesis and implications for Phanerozoic continental crustal growth. Lithos, 2010, 283–306
13 Davis G A, Wang C, Zheng Y D, et al. The enigmatic Yinshan fold and thrust belt northern China: New view on its intraplate contractional styles. Geology, 1998, 26: 43–46
14 Davis G A, Zheng Y D, Wang C, et al. Mesozoic tectonics on Hebei and Liaoning Provinces, Northern China. GSA Memoir, 2001, 194: 171–197
15 Hu J M, Liu X W, Xu G, et al. The Zhangyingzi-Liugou strike-slip fault in the Chengde area of Northern Hebei province and its tectonic significance (in Chinese). Geol Rev, 2005, 51: 621–632
16 Zhao Y. The Mesozoic Orogenies and tectonic evolution of the Yanshan area (in Chinese). Geol Rev, 1990, 36: 1–12
17 Cui S Q, Wu Z H. On the Mesozoic and Cenozoic intracontinental orogenesis of the Yanshan area, China (in Chinese). Proceedings of the 30th International Geological Congress. Beijing: Geological Publishing House, 1998. 216–228
18 Hu L, Song H L, Yan D P, et al. The The $^{40}Ar/^{39}Ar$ geochronology constraint and geological significance of mylonites in Shangyi-Chicheng fault belt on the north of North China Craton. Sci China Earth Sci, 2003, 11: 1134–1141
19 Wang Y. Magmatic thermal events and tectonic evolution of orogenic processes in inner Mongolia-Yanshan Orogenic Belt during end of late Paleozoic-Mesozoic (in Chinese). Geoscience, 1996, 10: 66–75
20 Liu W, Yang J H, Li C F, et al. Thermochronology of three major faults in the Chifeng area, Inner Mongolia of China (in Chinese). Acta Petrol Et Mineral, 2003, 19: 717–728
21 Wang Y B, Han J, Li J B. Age, petrogenesis and geological significance of the deformed granitoids in the Louzidian metamorphic core complex, southern Chifeng, InnerMongolia: Evidence from zircon U-Pb dates and Hf isotopes (in Chinese). Acta Petrol Et Mineral, 2010, 29: 763–778
22 Liu S W, Santosh M, Wang W, et al. Zircon U-Pb chronology of the Jianping Complex: Implications for the Precambrian crustal evolution history of the northern margin of North China Craton. Gondwana Res, 2011, 20: 48–63
23 Jia W. Found of migmatitic granite in Lamadong Chifeng, Inner Mongolia (in Chinese). Geol Inner Mongolia, 1999, 1: 29–33
24 Li Y G, Zhai M G, Miao L C, et al. Relationship between intrusive rocks and gold mineralization of the Anjiayingzi gold deposit, Inner Mongolia and its implications for geodynamics (in Chinese). Acta Petrol Et Mineral, 2003, 19: 808–816
25 Ouyang Z X. Comparision of geoehronology and origin of the late Mesozoie granitoids from major metamorphic core complexes in the North China craton and their significance (in Chinese). Dissertation for the Master's Degree. Beijing: Chinese Academy of Geologieal Seience, 2010. 1–205
26 Zhang Z. Permian to Triassic magmatism in the northern margin of the North China Craton (in Chinese). Dissertation for the Master's Degree. Beijing: Institute of Geology and Geophysics, Chinese Academy of Sciences, 2011. 1–100
27 Wang X S, Zheng Y D, Jia W. Extensional stages of Louzidian metamorphic core complex and development of the supradetachment basin south of Chifeng, Inner Mongolia, China. Acta Geo Sin-Engl, 2004, 78: 237–245
28 Zhang X H, Li T S, Pu Z P, et al. ^{40}Ar-^{39}Ar ages of Louzidian-Dachengzi ductile shear zone in Chifeng, Inner Mongolia and its tec-

tonic significance. Chin Sci Bull, 2002, 47: 951–956
29 Wang X S, Zheng Y D. $^{40}Ar/^{39}Ar$ age constraints on the ductile deformation of the detachment system of the Louzidian core complex, southern Chifeng, China (in Chinese). Geol Rev, 2005. 51: 574–582
30 Shao J A, Zhang L Q, Jia W, et al. Harkin metamorphic core complex in Inner Mongolia and its upwelling mechanism. Acta Petrol Et Mineral, 2001, 17: 283–290
31 Yuan H L, Gao S, Liu X M, et al. Accurate U-Pb age and trace element determinations of zircon by laser ablation inductively coupled plasma mass spectrometry. Geostand Geoanal Res, 2004, 28: 353–370
32 Liu Y S, Gao S, Hu Z C, et al. Continental and oceanic crust recycling-induced melt-peridotite interactions in the Trans-North China Orogen: U-Pb dating, Hf isotopes and trace elements in zircons from mantle xenoliths. J Petrol, 2010, 51: 537–571
33 Andersen T. Correlation of common lead in U-Pb analyses that do not report ^{204}Pb. Chem Geol, 2002, 192: 59–79
34 Zhang C H , Li C M, Deng H L, et al. Mesozoic contraction deformation in the Yanshan and northern Taihang Mountains and its implications to the destruction of the North China Craton. Sci China Earth Sci, 2011, 54: 798–822
35 Davis G A, Qian X L, Zheng Y D, et al. Mesozoic deformation and plutonism in the Yunmengshan: A Chinese metamorphic core complex north of Beijing, China. In: Yin A, Harrison T M, eds. The Tectonic Evolution of Asia. New York: Cambridge University Press, 1996. 253–280
36 Zhao Y, Zhang S H, Xu G, et al. The Jurassic major tectonic events of the Yanshanian intraplate deformation belt (in Chinese). Geol Bull Chin, 2004, 23: 854–863
37 Dong S W, Zhang Y Q, Long C X, et al. Jurassic tectonic revolution in China and new interpretation of the Yanshan movement (in Chinese). Acta Geol Sin, 2007, 81: 1449–1461
38 Zhang Y Q, Dong S W, Zhao Y, et al. Jurassic tectonics of North China: A synthetic view (in Chinese). Acta Geol Sin, 2007, 81: 1462–1480
39 Li S G, Hart S R, Zheng S G, et al. Timing of collision between the North and South China Blocks: The Sm-Nd isotopic age evidence. Sci China Ser B, 1989, 32: 1393–1400
40 Li S G, Huang F, Li H. Post-collisional lithosphere delamination of the Dabie-Sulu orogen. Chin Sci Bull, 2002, 47: 259–263
41 Zheng Y F. A perspective view on ultrahigh-pressure metamorphism and continental collision in the Dabie-Sulu orogenic belt. Chin Sci Bull, 2008, 53: 3081–3104
42 Zhu G, Liu G S, Niu M L, et al. Syn-collisional transform faulting of the Tan-Lu fault zone, East China. Int J Earth Sci (Geol Rundsch), 2009, 98: 135–155
43 Liu S F, Zhang G W, Cheng X Y, et al. Evolution of flexural basins and process of collision orogeny in east Qinling-Dabieshan and its adjacent regions (in Chinese). Sci Geol Sin, 1999, 34: 336–346
44 Yan G H, Mu B L, Xu B L, et al. Geochronology and isotopic features of Sr, Nd, and Pb of the Triassic alkali intrusions in the Yanshan-Yinshan regions. Sci China Earth Sci, 2000, 30: 383–387
45 Shao J A, Zhang L Q. Mesozoic dyke swarms in the north of North China (in Chinese). Acta Petrol Et Mineral, 2002, 18: 312–318